ACS OMEGA

http://pubs.acs.org/journal/acsodf

Article

Enhancement of Hydrothermal Stability and CO_2 Adsorption of Mg-MOF-74/MCF Composites

Chunling Xin,* Yang Ren, Zhaofei Zhang, Lili Liu, Xia Wang,* and Jinmei Yang

Cite This: *ACS Omega* 2021, 6, 7739−7745

Read Online

ACCESS | Metrics & More | Article Recommendations

ABSTRACT: Hierarchical porous composite Mg-MOF-74/MCFs were successfully synthesized using a simple and facile method under *in situ* solvothermal conditions. Textural structures and morphologies of the composites were characterized by X-ray diffraction (XRD), N_2 adsorption−desorption isotherms, and scanning electron microscopy (SEM), transmission electron microscopy (TEM), and thermogravimetric analysis (TGA). The results demonstrate that a large amount of nanosized Mg-MOF-74 particles is incorporated into the pores of mesocellular siliceous foams (MCFs) without remarkable aggregation and the composites possess microporous and mesoporous characteristics of both components. In addition, CO_2 adsorption properties of the composites were tested in a fixed bed with/without hydrothermal treatment. The total CO_2 adsorption capacities were calculated by breakthrough curves. The CO_2 adsorption capacity of the composites reaches 1.68 mmol/g, which is smaller than that of pristine Mg-MOF-74. However, the total CO_2 adsorption capacity of the composites after hydrothermal treatment reaches 2.66 mmol/g, which is larger than that of Mg-MOF-74 (2.39 mmol/g) under the same condition. XRD patterns and SEM images of the composites demonstrate that the hydrothermal stability and CO_2 adsorption performance of the composites were improved compared with those of pristine Mg-MOF-74 after hydrothermal treatment.

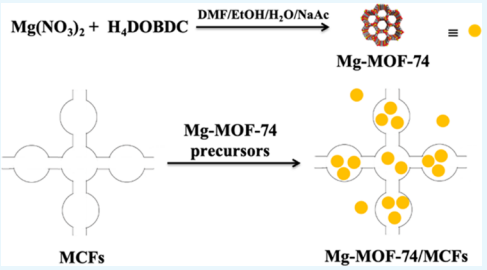

1. INTRODUCTION

Metal−organic frameworks (MOFs) are one of the most rapidly growing categories of crystalline porous materials with extremely large specific areas and tunable chemical functionalities, which provide promising prospect in the gas adsorption and separation area.[1] However, lower hydrothermal stability limits its practical applications.[2] Recently, a new strategy is proposed to the complete functional properties of the MOFs by hybridizing them with different active species like metal nanoparticles,[3] polyoxometalates,[4] graphene oxide (GO),[5,6] carbon nanotubes (CNTs),[7] and mesoporous materials.[8] Such composite materials can show better properties than the individual parent material.[9,10] For example, Bandosz et al. synthesized new composites combining MOFs with GO, and new porosity resulted from the synergistic effect of MOFs and GO.[10] The additional porosity is responsible for the enhancement of hydrogen uptake of the composites compared to the ones calculated for the physical mixture of HKUST-1 and GO. Ewa et al. successfully introduced MOFs into the core of multiwalled carbon nanotubes (MWCNTs). It was found that MOFs-5 confined to MWCNT interiors exhibit structure stability in atmospheric humidity for more than 3 days.

Ordered mesoporous silica is a series of porous siliceous materials with a large surface area and ordered porous structure.[11] The combination of mesoporous silica and microporous MOFs is beneficial for enhancing the lower chemical and mechanical stabilities of MOFs. Zhou et al. have incorporated MOFs into ordered mesoporous SiO_2, making MOFs well dispersed in silica nanopores.[12] Moreover, the thermal stability of MOFs was enhanced upon their incorporation into silica nanopores. Levan et al.[8] impregnated MOFs into the pore channel of MCM-41, which enhanced the hydrothermal stability of the MOFs. However, long one-dimensional (1D) cylinder pore channels, such as SBA-15 and MCM-4, are difficult for the diffusion of molecules.[13]

Mesocellular foam (MCF) is amorphous silica with high surface area and well-defined, uniform spherical pores (typically 20−45 nm) that are interconnected by cylindrical windows (8−25 nm).[14] The mesopore size of MCF is known to be larger than that of ordered mesoporous silica, such as MCM-41 and SBA-15,[11,15,16] providing more favorable conditions for mass diffusion. Therefore, MCFs were chosen as the substrate to prepare microporous/mesoporous composites.

Mg-MOF-74,[17] also denoted CPO-27, has 1D hexagonal channels of around 11−12 Å and a very high density of open

Received: January 8, 2021
Accepted: February 26, 2021
Published: March 11, 2021

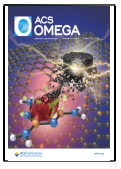

https://dx.doi.org/10.1021/acsomega.1c00098
ACS Omega 2021, 6, 7739−7745

metal sites after removal of coordinated water molecules. Previous reports demonstrated that Mg-MOF-74 has a high CO_2 affinity at subatmospheric pressure. Caskey found that the CO_2 adsorption capacity of MOF-74 reached 7.23 mmol/g at low CO_2 pressures (0.15 bar).[18] Besides, the exit of water vapor always inhibits the CO_2 adsorption performance of Mg-MOF-74.[19] In a real industrial process, the adsorbent is under the form of aggregated crystals called pellets. Hence, the MOF-74 powder needs to be shaped into pellets or extrudes of stable aggregated crystals.[20] However, this procedure is cumbersome for MOFs. Hence, MCFs were introduced into the Mg-MOF-74 precursor to synthesize Mg-MOF-74/MCF composites in our study. We studied synthesis, characterization, and CO_2 adsorption performance of MOF-74/MCF materials under simulated flue gas. The CO_2 adsorption capacity of the composites after hydrothermal treatment was also carried out on a fixed bed to estimate the hydrothermal stability of the composites.

2. RESULTS AND DISCUSSION

The XRD patterns of as-synthesized Mg-MOF-74 and Mg-MOF-74/MCFs are shown in Figure 1. As we can see that two

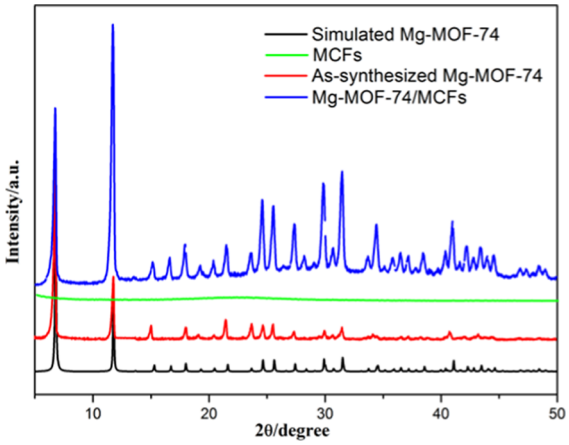

Figure 1. XRD patterns of simulated Mg-MOF-74, as-synthesized Mg-MOF-74 MCFs, and Mg-MOF-74/MCFs.

featured diffraction peaks located at Bragg angle 2θ of 6.7 and 11.7° well correspond to the simulated Mg-MOF-74. The results suggest that the crystalline structure of Mg-MOF-74 in the composites is not affected by the introduction of MCFs. Meanwhile, the broad diffraction peak between 15 and 35° corresponding to MCFs in Mg-MOF-74/MCFs also illustrates the amorphous structure of mesoporous silica particles.[21]

To study the textual properties of Mg-MOF-74, MCFs, and Mg-MOF-74/MCFs, N_2 adsorption isotherms were measured at 77 K. As shown in Figure 2, Mg-MOF-74 exhibits a type I isotherm, which is attributed to the characteristics of the microporous structure. Mg-MOF-74/MCFs possess a combination of type I and type IV isotherms, characteristics of microporous materials and mesoporous materials. Hence, the composites demonstrate the presence of additional mesopores resulting from MCFs except for the micropores of pristine Mg-MOF-74. The Brunauer–Emmett–Teller (BET) specific area of Mg-MOF-74/MCFs reaches 657.75 m^2/g, which is larger than that of Mg-MOF-74 (Table 1). Due to the cylindrical

Table 1. Textual Properties of Mg-MOF-74 and Mg-MOF-74/MCFs

sample	BET specific area (m^2/g)	pore size (nm)	pore volume (cm^3/g)
Mg-MOF-74	494.77	0.77[c]	0.22
Mg-MOF-74/MCFs	655.75	0.78[c], 18.4[a], 30.8[b]	0.50
MCFs	702.34	18.5[a], 30.8[b]	2.44

[a]Window size of MCFs is determined from the desorption branch. [b]Cell size of MCFs is determined from the adsorption branch. [c]Pore size of Mg-MOF-74 is determined according to Horvath–Kawazoe method.

pore geometry of Mg-MOF-74, the pore size distribution of Mg-MOF-74 was estimated according to the Horvath–Kawazoe method, as shown in Figure 2. It can be found that the median pore size of Mg-MOF-74 was 0.77 nm, which was in accordance with the adsorption–desorption isotherm. The pore size distribution of Mg-MOF-74/MCF composites was estimated according to the BJH method; the window pore size and the cell pore size of MCFs were estimated according to the desorption and adsorption branch isotherms, respectively. The window pore size and cell pore size of MCFs in the composite were 18.4 and 30.8 nm, respectively, which are similar to the window pore size and cell pore size of MCFs. The larger pore

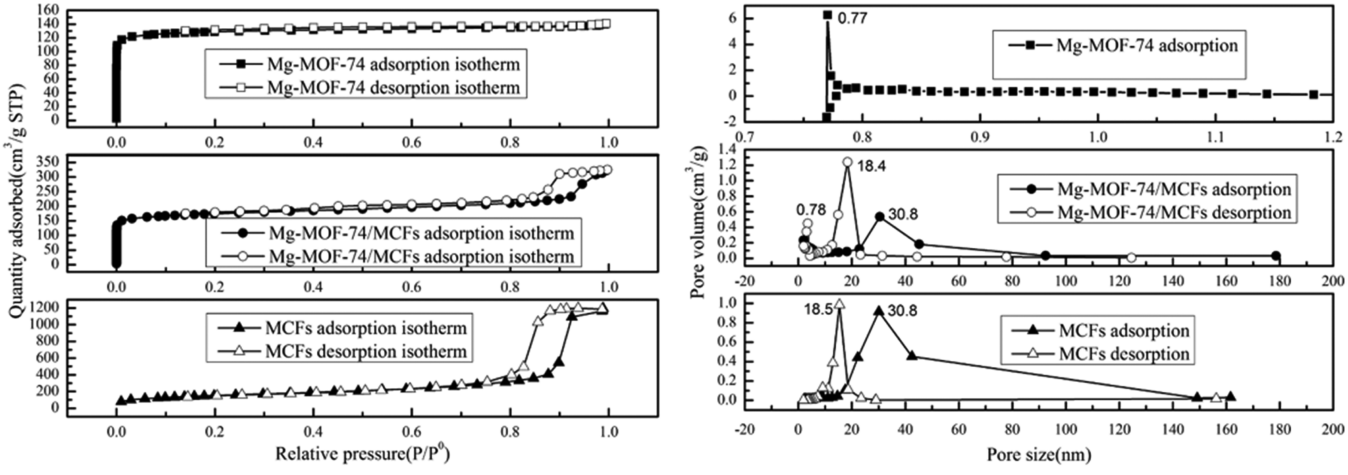

Figure 2. N_2 adsorption and desorption isotherms and pore size distribution of Mg-MOF-74, MCFs, and Mg-MOF-74/MCFs.

https://dx.doi.org/10.1021/acsomega.1c00098
ACS Omega 2021, 6, 7739–7745

size of MCFs is beneficial for the diffusion of Mg-MOF-74 precursor molecules. The pore volume of Mg-MOF-74/MCFs is smaller than that of MCFs, which may be because nanosized Mg-MOF-74 was encapsulated into the pore of MCFs.

The loading amount of Mg-MOF-74 in the composites is calculated from the thermogravimetric analysis (TGA) profiles. Compared with the activated Mg-MOF-74 profile, a large weight loss was observed between 100 and 300 °C, which is due to the loss of solvent embedded in the frameworks of Mg-MOF-74. The loading amount results from the weight loss of dried Mg-MOF-74 at 250 °C since MCFs do not show any weight loss at 250 °C according to the TGA profile of MCFs.[22] Here, the loading amounts of Mg-MOF-74 in the composite were calculated using as-synthesized Mg-MOF-74 and Mg-MOF-74/MCFs. As shown in Figure 3, the weight loss of dried

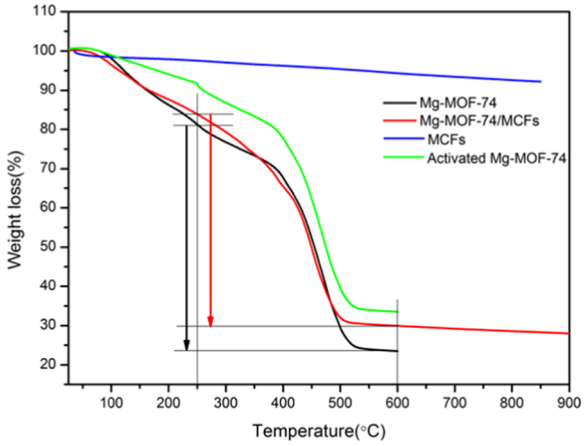

Figure 3. TGA profiles of Mg-MOF-74, MCFs, activated Mg-MOF-74, and Mg-MOF-74/MCFs.

Mg-MOF-74 is 57% at 250 °C, while the weight loss of the composites at 250 °C is 54%. Hence, the loading amount of Mg-MOF-74 in the composites is estimated to be 93% (54/57).

To study the effect of MCFs on the morphology of Mg-MOF-74, scanning electron microscopy (SEM) and transmission electron microscopy (TEM) analyses of samples were carried out. As shown in Figure 4a, Mg-MOF-74 crystals show a needle shape with a length of ∼1.5 μm aggregated to cauliflower morphology. Meanwhile, Mg-MOF-74/MCFs present the same morphology as MCF particles with nanosized particles loaded on the surface of MCFs (Figure 4b). Energy-dispersive X-ray spectroscopy (EDX) analyses of Mg-MOF-74/MCFs show the presence of Mg and Si elements, which results from Mg-MOF-74 and MCFs, respectively. From the SEM images, it is difficult to illustrate that Mg-MOF-74 nanoparticles encapsulate into the pores of MCFs. To clearly prove the sites of Mg-MOF-74 nanoparticles, TEM images of MCFs and Mg-MOF-74/MCFs were recorded. As can be seen from Figure 5, the MCF particles were ∼29 nm in cell pore diameter with significant and uniform porosity, which is in accordance with BJH pore size distribution. MCF particles possess a disordered array of silica struts, which is the characteristic structural feature of the MCFs.[23] From the TEM images of Mg-MOF-74/MCF composites, it can be found that nanosized Mg-MOF-74 crystals were encapsulated into the pores of MCFs, even though without even distribution. Thus, Mg-MOF-74 crystals can be immersed in the pores of MCFs using the synthesis procedure. Some Mg-MOF-74 nanoparticles were distributed on the outside of MCFs, which may have resulted from the small amounts of MCFs used in the synthesis of the composites. It can increase the amount of MCFs in the synthesis of the composites to decrease the amount of Mg-MOF-74 distributed outside of MCFs.

In the growth process of the composites, MCFs play an important role in the nucleation of Mg-MOF-74. The presence of silanol groups of MCFs has a stronger affinity to the precursor of Mg-MOF-74 crystals. Here, MCFs act as a microsized reactor for the growth of Mg-MOF-74. The synthesis strategy of the composites relies on the facile diffusion of the Mg-MOF-74 precursor molecules, so the larger pore size of MCFs is beneficial to the diffusion of MOF precursor molecules.

To evaluate the practical application of the hybrid Mg-MOF-74/MCFs for adsorbing CO_2 in the flue gas, we conducted dynamic breakthrough experiments in a fixed-bed reactor with binary gas (CO_2/N_2 = 10:90%) simulated a flue gas at 30 °C. All of the samples were activated at 200 °C before adsorption experiments. The breakthrough curves of all of the composites and desolvated Mg-MOF-74 are shown in Figure 6. As we can see from the dynamic breakthrough curves, the breakthrough time of the composite is shifted right compared to Mg-MOF-74, which suggests that the adsorption capacity of the composite is increased remarkably. The total CO_2 adsorption capacities of the composite and MOFs crystals are calculated according to equation (1-1), which are listed in Table 2. The total CO_2 adsorption capacities of Mg-MOF-74 and Mg-MOF-74/MCFs are 3.70 and 1.68 mmol/g, respectively. Here, the total CO_2 adsorption capacity of MCFs is 0.45 mmol/g. The presence of MCFs in the composites leads to decreased CO_2 adsorption capacity compared to that of pristine Mg-MOF-74. However, the exit of mesoporous MCFs increases the gas molecule diffusion rate. As we can see from Figure 7, here, M_t is the CO_2 adsorption capacity at time t and M_e is the CO_2 adsorption capacity at equilibrium. The result shows that the adsorption rate of Mg-MOF-74/MCFs is larger than that of Mg-MOF-74. The increase of adsorption kinetics in the composite may be due to an increase in molecular diffusivity in the nanoparticles as well as the mesopores (Figure 8).

Since flue gases always contain 8−17 vol % water vapor, a promising adsorbent should have excellent hydrothermal stability in practical applications. The dynamic adsorption capacity of the composite after hydrothermal treatment was also conducted in a fixed-bed reactor. The results are shown in Table 2, which suggests that the CO_2 adsorption capacity of conditioned Mg-MOF-74/MCFs is 2.66 mmol/g larger than that of conditioned Mg-MOF-74 (2.39 mmol/g). It may be due to CO_2 molecules dissolving in the water adsorbed in the framework of MCFs after hydrothermal treatment. Furthermore, the CO_2 adsorption capacity of conditioned composites is larger than that of untreated composites because a certain amount of hydroxyl groups of MCFs that disappeared in the calcination process have reformed after hydrothermal treatment,[24] hence a reduction in water vapor adsorption capacity compared to CO_2 in Mg-MOF-74 of the composites. As we can see from Figure 9, the diffraction peaks located at 2θ of 11.7° of Mg-MOF-74 decrease dramatically after hydrothermal treatment, which suggests that the structures of Mg-MOF-74 collapsed to a certain extent by hydrothermal treatment. Meanwhile, even the reduction of diffraction peaks intensity of

https://dx.doi.org/10.1021/acsomega.1c00098
ACS Omega 2021, 6, 7739−7745

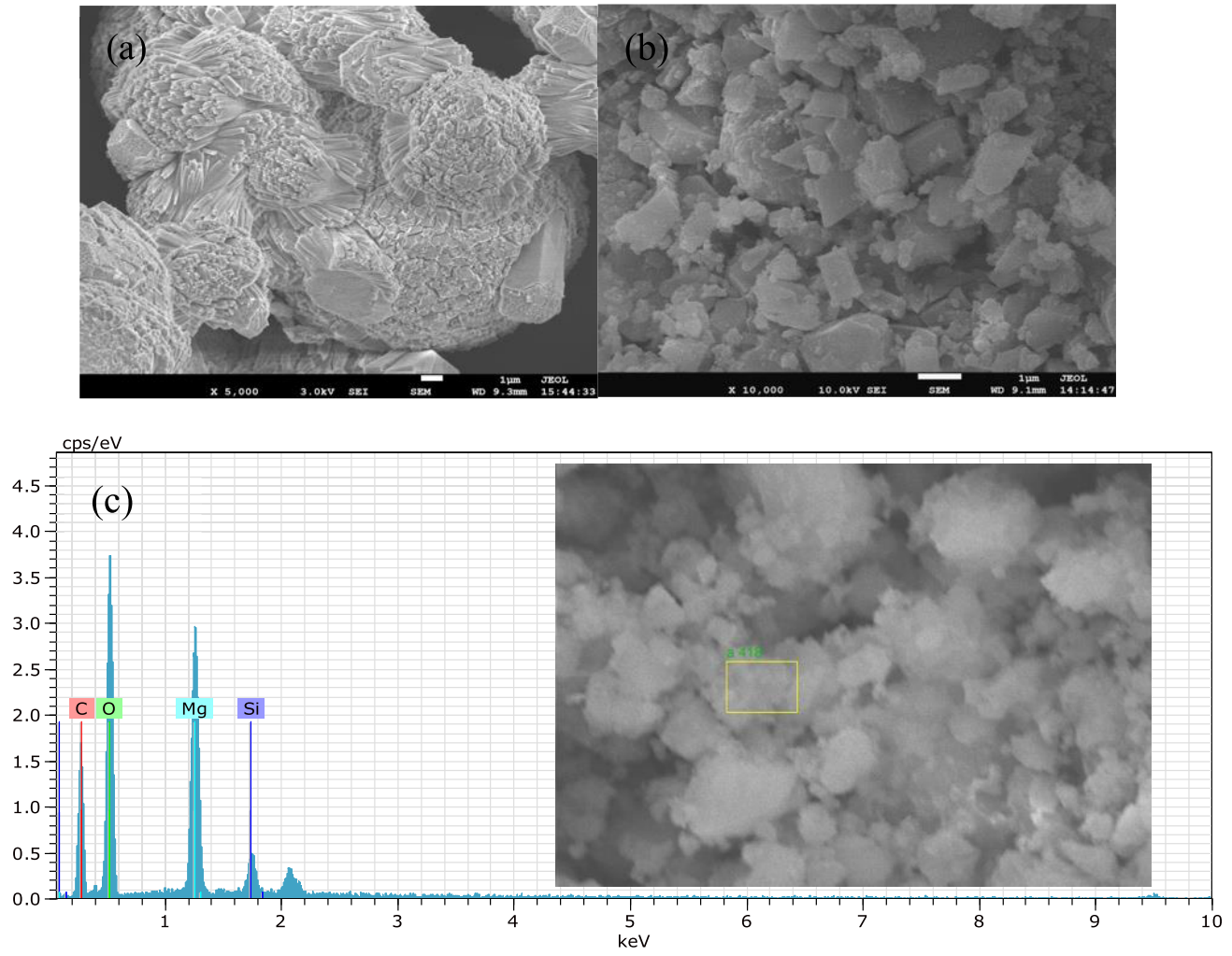

Figure 4. SEM images of Mg-MOF-74 (a) and Mg-MOF-74/MCFs (b). EDX spectrum of Mg-MOF-74/MCFs (c).

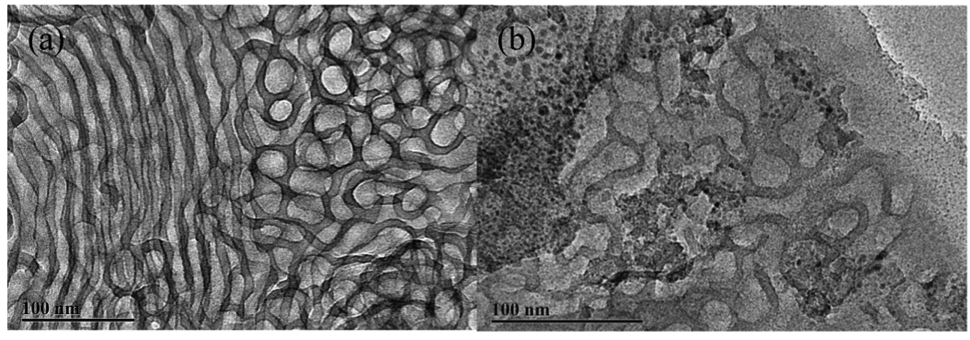

Figure 5. TEM images of MCFs (a) and Mg-MOF-74/MCFs (b).

Mg-MOF-74 in the composites due to the loading amounts of MOFs, no changes in intensity of diffraction peaks of Mg-MOF-74 in the composites after hydrothermal treatment. The results illustrate that the introduction of MCFs can improve the hydrothermal stability of Mg-MOF-74.

To further illustrate that the hydrothermal stability of Mg-MOF-74/MCFs, N_2 adsorption and desorption isotherms of MCFs, Mg-MOF-74, and Mg-MOF-74/MCFs were examined. The detailed textural properties of all samples are listed in Table 3. As we can see from Table 3, the BET specific area of Mg-MOF-74 decreases remarkably after hydrothermal treatment, while the S_{BET} of Mg-MOF-74/MCFs after hydrothermal treatment is higher than that of the composite without any treatment. The results further prove that the introduction of MCFs improves the hydrothermal stability of Mg-MOF-74 in Mg-MOF-74/MCFs.

In practical applications, regenerability is an important factor to consider for the solid adsorbent. Therefore, CO_2 adsorption−desorption cycles were conducted to measure the regenerability of the composite. The results shown in Figure 10 illustrate that the CO_2 adsorption capacity remained unchanged after ten cycles. At the same time, the CO_2 adsorption capacity of Mg-MOF-74 decreased gradually.

https://dx.doi.org/10.1021/acsomega.1c00098
ACS Omega 2021, 6, 7739−7745

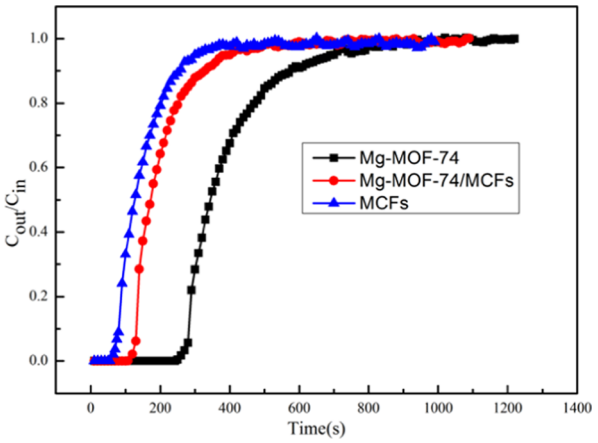

Figure 6. Dynamic breakthrough curves of Mg-MOF-74, MCFs, and Mg-MOF-74/MCFs at 30 °C.

Table 2. CO_2 Adsorption Capacity of All of the Samples before and after Hydrothermal Treatment

	total CO_2 adsorption capacity (mmol/g)	
samples	initial	conditioned
Mg-MOF-74	3.70	2.39
Mg-MOF-74/MCFs	1.68	2.66
MCFs	0.45	0.64

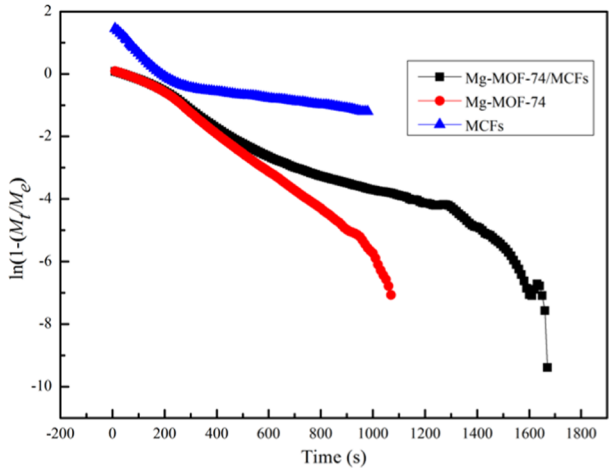

Figure 7. CO_2 adsorption kinetics profiles on Mg-MOF-74, MCFs, and Mg-MOF-74/MCFs at 303 K.

Hence, the Mg-MOF-74/MCF composite is a promising adsorbent in practical applications.

3. EXPERIMENTAL SECTION

3.1 Chemicals. Magnesium nitrate hexahydrate ($Mg(NO_3)_2{\cdot}6H_2O$, 99%), 2,5-dihydroxyterphthalic acid (H_4DOBDC, 98%), *N*,*N*-dimethylformamide (DMF, 99.5%), triethylamine (TEA, 99%), and ethanol (EtOH, 99.7%) were purchased from Aladdin Industrial Corporation. Deionized water is made by the laboratory.

3.2. Synthesis of Mg-MOF-74. Mg-MOF-74 was synthesized according to the previous report with little modifications.[17] The detailed synthesis process is described as follows: 0.111 g of 2,5-dihydroxyterphthalic acid (H_4DOBDC) and 0.475 g of magnesium nitrate ($Mg(NO_3)_2{\cdot}6H_2O$) were dissolved in 50 mL of a mixed solution

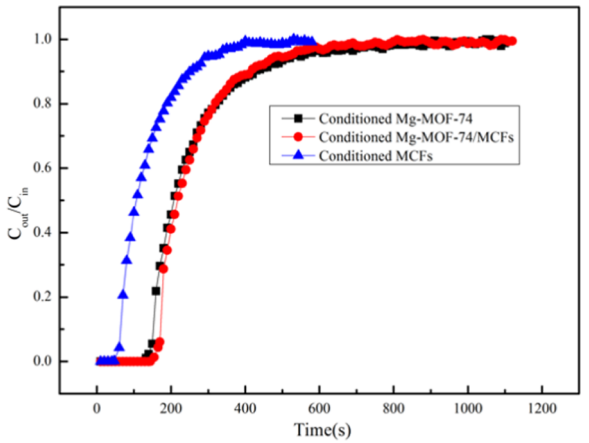

Figure 8. Total CO_2 adsorption capacity of Mg-MOF-74, MCFs, and Mg-MOF-74/MCFs after hydrothermal pretreatment.

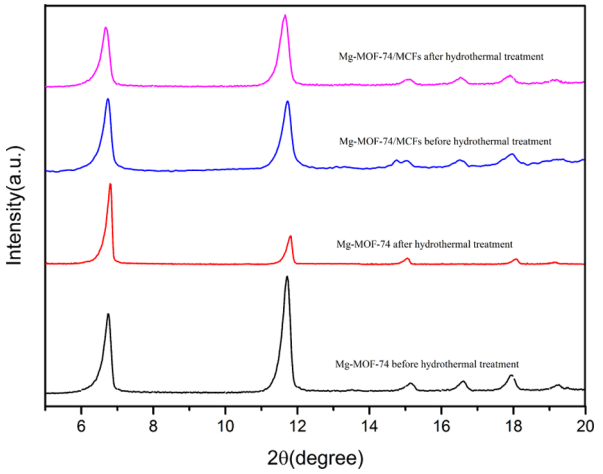

Figure 9. XRD patterns of Mg-MOF-74 and Mg-MOF-74 before and after hydrothermal treatment.

Table 3. Textural Properties of MCFs, Mg-MOF-74, and Mg-MOF-74/MCFs after Hydrothermal Treatment

sample	S_{BET} (m^2/g)	total pore volume (cm^3/g)
Mg-MOF-74	275.67	0.14
Mg-MOF-74/MCFs	521.45	0.36
MCFs	579.23	1.89

of *N*,*N*-dimethylformamide (DMF), ethanol, and deionized water (H_2O) (15:1:1, v/v/v). TEA (0−0.16 mL) was slowly added to the mixed solution. The mixed solution was sealed in the vial and heated at 125 °C for 20 h in a convection oven. The obtained yellow crystals were washed with DMF three times and placed in methanol, which was decanted and replenished four times in 3 days. Finally, the solvent was removed, and the as-synthesized crystals were dried at 100 °C overnight. TEA was adopted as a deprotonation reagent, and the obtained crystals were denominated as Mg-MOF-74.

3.3. Synthesis of Mg-MOF-74/MCFs. MCFs were synthesized according to the previous report.[25] MCFs (0.5 g) were added to the precursor solution of Mg-MOF-74 and stirred at room temperature for 6 h. TEA (0−16 mL) was slowly added to the mixed solution. The mixed solution was sealed in the vial and heated at 125 °C for 20 h in the convection oven. Finally, the obtained samples were washed

https://dx.doi.org/10.1021/acsomega.1c00098
ACS Omega 2021, 6, 7739−7745

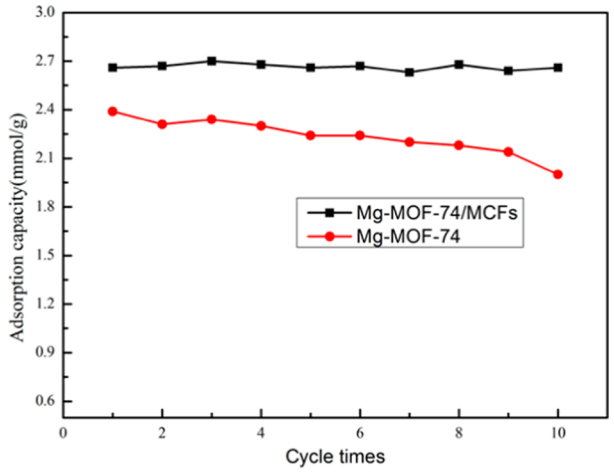

Figure 10. CO_2 adsorption capacity of Mg-MOF-74 and Mg-MOF-74/MCFs after hydrothermal treatments for ten CO_2 adsorption−desorption cycles.

with DMF and placed in methanol, which was decanted and replenished four times in 3 days. Finally, the solvent was removed, and the as-synthesized crystals were dried at 100 °C overnight. The obtained sorbents were denoted as Mg-MOF-74/MCFs.

3.4. CO_2 Dynamic Breakthrough Experiment. CO_2 adsorption and desorption processes were conducted in a fixed-bed reactor. Moderate adsorbents were added in a U-type quartz tube with an inner diameter of 8 mm and plugged by quartz wool in the side of the gas outlet. The adsorbents were pressed into a disk under 5 MPa for 3 min, and then, the disk was broken into particles and the particles were sieved to obtain 20−40 mesh particles. The sorbents were activated at 200 °C for 6 h in an argon atmosphere with a flow of 60 mL/min and then cooled to adsorption temperature under the argon atmosphere. The simulated flue gases (CO_2 10 vol %, N_2 90 vol %) were introduced into the reactor. The CO_2 concentration of the outlet gas of the quartz tube was determined by a gas analyzer (Vaisala, Finland) for every 10 s. The CO_2 adsorption capacity of adsorbents can be determined from the breakthrough curves, as reported in the previous report.[26] The values are calculated according to the following equations:

$$q = \frac{C_0 V t_s}{22.4W} \quad (1)$$

$$t_s = \int_0^t \left(1 - \frac{C_t}{C_0}\right) d_t \quad (2)$$

where t_s is the dead time (s), C_0 is the feed gas concentration, W is the weight of the activated adsorbent (g), V is the volumetric flow rate (mL/min), q is the equilibrium adsorption capacity of the adsorbent (mmol/g), C_t is the outlet gas concentration, and t is the adsorption time (s).

3.5. Hydrothermal Treatment. To estimate the hydrothermal stability of Mg-MOF-74 and its composites at high temperature and humidity conditions, all of the adsorbents were placed on filter papers and suspended above a beaker filled with 85 °C hot water for 2 h. After hydrothermal treatment, the samples were dried at room temperature.

3.6. Characterization. Powder X-ray diffraction (PXRD) patterns were collected with a D8 Advanced diffractometer operated at 40 kV and 40 mA with monochromated Cu Kα radiation (λ = 1.5406 Å) and at a scan speed of 3°/min. The simulated PXRD patterns were calculated from modeled crystal data using the Diamond 3.2i software suite. Nitrogen sorption isotherms were measured at 77 K on a Micromeritic ASAP 2020 system. The samples were outgassed at 473 K overnight before the measurement. Scanning electron microscopy (SEM) images were obtained on a JEOL at 10 kV. Before measurements, the samples suspended in the ethanol were dropped onto a tin-foil plate and dried at room temperature. Transmission electron microscopy (TEM) investigations were performed with a JEM-2100F (operated at 10 kV). Before the measurement, the material was deposited onto a holey carbon foil supported on a copper grid. Thermogravimetric analysis (TGA) was performed on a Rigaku TG thermal gravimetric analyzer in the temperature range of 30−700 °C under a nitrogen atmosphere at a heating rate of 10 °C/min.

4. CONCLUSIONS

Mg-MOF-74/MCF hybrid composites were synthesized by a simple and facile route by dispersing MCFs into the Mg-MOF-74 precursors. The larger pore size of MCFs makes it easy for the diffusion of MOF precursor molecules into the cell of MCFs. The hybrid composites possess binary characteristics of both components. Besides, the adsorption kinetics of the composites is enhanced due to an increase in molecular diffusivity in the nanoparticles as well as mesopores. Mg-MOF-74/MCFs exhibit interesting CO_2 adsorption behaviors due to the presence of MCFs. This may be due to the reformation of hydroxyl groups in MCFs in the moisture environment, thus decreasing the competitive adsorption of water vapor in Mg-MOF-74 compared to CO_2. After hydrothermal treatment, the composites show an increase in dynamic CO_2 adsorption performance. After ten CO_2 adsorption−desorption cycles, the CO_2 adsorption capacity remains unchanged. Therefore, it is promising for the composites acting as solid adsorbents in practical applications.

AUTHOR INFORMATION

Corresponding Authors

Chunling Xin − *Department of Chemistry and Chemical & Environmental Engineering, Weifang University, Weifang 261061, China;* orcid.org/0000-0002-1496-1262; Email: xinchunling0925@126.com

Xia Wang − *Department of Chemistry and Chemical & Environmental Engineering, Weifang University, Weifang 261061, China;* orcid.org/0000-0003-2651-7166; Email: xiawangwfu@163.com

Authors

Yang Ren − *Department of Chemistry and Chemical & Environmental Engineering, Weifang University, Weifang 261061, China*

Zhaofei Zhang − *LUXI Group Co., Ltd., Liaocheng 252211, China*

Lili Liu − *Department of Chemistry and Chemical & Environmental Engineering, Weifang University, Weifang 261061, China;* orcid.org/0000-0002-3062-0783

Jinmei Yang − *Department of Chemistry and Chemical & Environmental Engineering, Weifang University, Weifang 261061, China*

Complete contact information is available at: https://pubs.acs.org/10.1021/acsomega.1c00098

https://dx.doi.org/10.1021/acsomega.1c00098
ACS Omega 2021, 6, 7739−7745

Notes

The authors declare no competing financial interest.

■ ACKNOWLEDGMENTS

The project was supported by the National Natural Science Foundation of China (21802104) and the Natural Science Foundation of Shandong Province (ZR2018QEM003).

■ REFERENCES

(1) Ahmed, I.; Khan, N. A.; Jhung, S. H. Graphite Oxide/Metal-Organic Framework (MIL-101): Remarkable Performance in the Adsorptive Denitrogenation of Model Fuels. *Inorg. Chem.* **2013**, *52*, 14155−14161.

(2) Qian, D.; Lei, C.; Hao, G. P.; Li, W. C.; Lu, A. H. Synthesis of hierarchical porous carbon monoliths with incorporated metal-organic frameworks for enhancing volumetric based CO_2 capture capability. *ACS Appl. Mater. Interfaces* **2012**, *4*, 6125−6132.

(3) Hermes, S.; Schröter, M.-K.; Schmid, R.; Khodeir, L.; Muhler, M.; Tissler, A.; Fischer, R. W.; Fischer, R. A. Metal@MOF: Loading of Highly Porous Coordination Polymers Host Lattices by Metal Organic Chemical Vapor Deposition. *Angew. Chem., Int. Ed.* **2005**, *44*, 6237−6241.

(4) Yan, A.-X.; Yao, S.; Li, Y.-G.; Zhang, Z.-M.; Lu, Y.; Chen, W.-L.; Wang, E.-B. Incorporating Polyoxometalates into a Porous MOF Greatly Improves Its Selective Adsorption of Cationic Dyes. *Chem. - Eur. J.* **2014**, *20*, 6927−6933.

(5) Petit, C.; Bandosz, T. J. MOF-Graphite Oxide Composites: Combining the Uniqueness of Graphene Layers and Metal-Organic Frameworks. *Adv. Mater.* **2009**, *21*, 4753−4757.

(6) Yang, J. H.; Yang, D.; Li, Y. M. Graphene supported chromium carbide material synthesized from Cr-based MOF/graphene oxide composites. *Mater. Lett.* **2014**, *130*, 111−114.

(7) Chen, X.; Lukaszczuk, P.; Tripisciano, C.; Rümmeli, M. H.; Srenscek-Nazzal, J.; Pelech, I.; Kalenczuk, R. J.; Borowiak-Palen, E. Enhancement of the structure stability of MOF-5 confined to multiwalled carbon nanotubes. *Phys. Status Solidi B* **2010**, *247*, 2664−2668.

(8) Furtado, A. M. B.; Liu, J.; Wang, Y.; Levan, M. D. Mesoporous silica-metal organic composite: synthesis, characterization, and ammonia adsorption. *J. Mater. Chem.* **2011**, *21*, 6698−6706.

(9) Chakraborty, A.; Maji, T. K. Mg-MOF-74@SBA-15 hybrids: Synthesis, characterization, and adsorption properties. *APL Mater.* **2014**, *2*, No. 124107.

(10) Petit, C.; Burress, J.; Bandosz, T. J. The synthesis and characterization of copper-based metal−organic framework/graphite oxide composites. *Carbon* **2011**, *49*, 563−572.

(11) Huo, Q.; Margolese, D. I.; Stucky, G. D. Surfactant Control of Phases in the Synthesis of Mesoporous Silica-Based Materials. *Chem. Mater.* **1996**, *8*, 1147−1160.

(12) Sun, L. B.; Li, J. R.; Lu, W.; Gu, Z. Y.; Luo, Z.; Zhou, H. C. Confinement of metal-organic polyhedra in silica nanopores. *J. Am. Chem. Soc.* **2012**, *134* (38), 15923−15928.

(13) Li, P.; Modica, J. A.; Howarth, A. J.; Vargas, E.; Moghadam, P. Z.; Snurr, R. Q.; Mrksich, M.; Hupp, J. T.; Farha, O. K. Toward Design Rules for Enzyme Immobilization in Hierarchical Mesoporous Metal-Organic Frameworks. *Chem* **2016**, *1*, 154−169.

(14) Lukens, W. W.; Schmidt-Winkel, P.; Zhao, D.; Feng, J.; Stucky, G. D. Evaluating Pore Sizes in Mesoporous Materials: A Simplified Standard Adsorption Method and a Simplified Broekhoff−de Boer Method. *Langmuir* **1999**, *15*, 5403−5409.

(15) Lettow, J. S.; Han, Y. J.; Schmidt-Winkel, P.; Yang, P.; Zhao, D.; Stucky, G. D.; Ying, J. Y. Hexagonal to Mesocellular Foam Phase Transition in Polymer-Templated Mesoporous Silicas. *Langmuir* **2000**, *16*, 8291−8295.

(16) Kruk, M.; Jaroniec, M.; Ko, C. H.; Ryoo, R. Characterization of the Porous Structure of SBA-15. *Chem. Mater.* **2000**, *12*, 1961−1968.

(17) Millward, A. R.; Yaghi, O. M. Metal−Organic Frameworks with Exceptionally High Capacity for Storage of Carbon Dioxide at Room Temperature. *J. Am. Chem. Soc.* **2005**, *127*, 17998−17999.

(18) Caskey, S. R.; Wong-Foy, A. G.; Matzger, A. J. Dramatic Tuning of Carbon Dioxide Uptake via Metal Substitution in a Coordination Polymer with Cylindrical Pores. *J. Am. Chem. Soc.* **2008**, *130*, 10870−10871.

(19) Yu, J.; Balbuena, P. B. Water Effects on Postcombustion CO_2 Capture in Mg-MOF-74. *J. Phys. Chem. C* **2013**, *117*, 3383−3388.

(20) Remy, T.; Peter, S. A.; Van der Perre, S.; Valvekens, P.; De Vos, D. E.; Baron, G. V.; Denayer, J. F. M. Selective Dynamic CO_2 Separations on Mg-MOF-74 at Low Pressures: A Detailed Comparison with 13X. *J. Phys. Chem. C* **2013**, *117*, 9301−9310.

(21) Zhai, Q.-Z.; Hu, W.-H.; Huang, B.-L.; Wang, C.-Y. Synthesis and characterization of mesoporous SBA-15/propranolol hydrochloride for controlled drug release study. *J. Sol-Gel Sci. Technol.* **2012**, *63*, 435−444.

(22) Lettow, J. S.; Lancaster, T. M.; Glinka, C. J.; Ying, J. Y. Small-Angle Neutron Scattering and Theoretical Investigation of Poly(ethylene oxide)−Poly(propylene oxide)−Poly(ethylene oxide) Stabilized Oil-in-Water Microemulsions. *Langmuir* **2005**, *21*, 5738−5746.

(23) Schmidt-Winkel, P.; Lukens, W. W.; Yang, P.; Margolese, D. I.; Lettow, J. S.; Ying, J. Y.; Stucky, G. D. Microemulsion Templating of Siliceous Mesostructured Cellular Foams with Well-Defined Ultralarge Mesopores. *Chem. Mater.* **2000**, *12*, 686−696.

(24) Xin, C.; Jiao, X.; Yin, Y.; Zhan, H.; Li, H.; Li, L.; Zhao, N.; Xiao, F.; Wei, W. Enhanced CO_2 Adsorption Capacity and Hydrothermal Stability of HKUST-1 via Introduction of Siliceous Mesocellular Foams (MCFs). *Ind. Eng. Chem. Res.* **2016**, *55*, 7950−7957.

(25) Xin, C.; Zhao, N.; Zhan, H.; Xiao, F.; Wei, W.; Sun, Y. Phase Transition of Silica in the TMB-P123-H_2O-TEOS Quadru-component System: A Feasible Route to Different Mesostructured Materials. *J. Colloid Interface Sci.* **2014**, *433*, 176−182.

(26) Xin, C.; Zhan, H.; Huang, X.; Li, H.; Zhao, N.; Xiao, F.; Wei, W.; Sun, Y. Effect of various alkaline agents on the size and morphology of nano-sized HKUST-1 for CO2 adsorption. *RSC Adv.* **2015**, *5*, 27901−27911.

https://dx.doi.org/10.1021/acsomega.1c00098
ACS Omega 2021, 6, 7739−7745